

Studies on the transport of high intensity laser-generated hot electrons in cone coupled wire targets

J. A. King,¹ K. U. Akli,² R. R. Freeman,^{3,4} J. Green,⁵ S. P. Hatchett,⁶ D. Hey,^{6,4} P. Jamangi,⁷ M. H. Key,⁶ J. Koch,⁶ K. L. Lancaster,⁵ T. Ma,¹ A. J. MacKinnon,⁶ A. MacPhee,⁶ P. A. Norreys,⁵ P. K. Patel,⁶ T. Phillips,⁶ R. B. Stephens,² W. Theobald,⁴ R. P. J. Town,⁶ L. Van Woerkom,³ B. Zhang,⁴ and F. N. Beg^{1,a)}

¹*Department of Mechanical and Aerospace Engineering, University of California San Diego, La Jolla, California 92093, USA*

²*General Atomics, San Diego, California 92186, USA*

³*Ohio State University, Columbus, Ohio 43210, USA*

⁴*Department of Applied Science, University of California, Davis, Livermore, California 94550, USA*

⁵*Rutherford Appleton Laboratory, Chilton, Oxon OX110QX, United Kingdom*

⁶*Lawrence Livermore National Laboratory, University of California, Livermore, California 94550, USA*

⁷*Laboratory for Laser Energetics, University of Rochester, Rochester, New York 14623, USA*

(Received 13 August 2008; accepted 8 January 2009; published online 3 February 2009)

Experimental results showing hot electron penetration into Cu wires using $K\alpha$ fluorescence imaging are presented. A 500 J, 1 ps laser was focused at $f/3$ into hollow aluminum cones joined at their tip to Cu wires of diameters from 10 to 40 μm . Comparison of the axially diminishing absolute intensity of Cu $K\alpha$ with modeling shows that the penetration of the electrons is consistent with one dimensional Ohmic potential limited transport. The laser coupling efficiency to electron energy within the wire is shown to be proportional to the cross sectional area of the wire, reaching 15% for 40 μm wires. Further, we find the hot electron temperature within the wire to be about 750 keV. The relevance of these data to cone coupled fast ignition is discussed. © 2009 American Institute of Physics. [DOI: 10.1063/1.3076142]

Fast ignition (FI) (Ref. 1) is a form of inertial confined fusion² that proposes to ignite a precompressed deuterium-tritium (DT) target by the use of a separate high intensity short pulse laser. Current designs call for the laser to be focused close to the compressed core via a hollow cone embedded within the target. Previous experiments^{3,4} have already shown that a hollow gold (Au) cone, despite involving complex physics, can provide a path through the low density plasma of an imploded capsule permitting hot electrons generated at the cone tip to heat efficiently the compressed plasma in small scale integrated tests of FI. Up to 20% coupling efficiency of laser energy transferred to thermal energy in the compressed plasma has been reported. This overall coupling efficiency determines the short pulse laser energy required for FI, but only in Ref. 4 quantitative data has been reported using imploded shells.

Wires attached to cones have been used to study the laser-plasma component of the overall coupling efficiency: the wire serves to collimate and guide the hot electron current for convenient detection and characterization of their number and temperature. Although the plasma temperature and densities in an integrated FI experiment⁵ will be significantly different than those in a wire,⁶ cone-wire experiments can help elucidate the physics of high intensity laser-plasma energy coupling.

In this letter, results from recent cone-wire experiments are presented. We observed the $K\alpha$ intensity distribution in the wire and used a one dimensional (1D) model to analyze

the distribution that depends on two parameters: the laser-to-wire energy coupling efficiency and the average value of T_{hot} . The “best fit” parameters indicate that up to 15% of the laser energy is coupled from an aluminum cone to a 40 μm diameter wire, and that the hot electron temperature in the wire is approximately 750 keV, less than that predicted by conventional ponderomotive scaling.⁷ We discuss the applicability of a simplified 1D fluid model for extraction of these parameters and note the connection to recent experimental results and computer modeling.

Experiments were performed at the Vulcan petawatt laser facility⁸ at the Rutherford Appleton Laboratory in the UK. Nd:glass (1053 nm) chirped pulse amplification (CPA) laser pulses were focused by an $f/3$ off-axis parabolic mirror into 1 mm long, 30° full angle, hollow Al cones [see Fig. 1(a)]. The average values of on-target laser energy and pulse duration were 345 ± 51 J and 1 ps. The laser focal spot pattern had a central peak of ~ 7 μm full width at half maximum containing $\sim 30\%$ of the energy giving peak intensity of 2.7×10^{20} W cm^{-2} . The wall thickness of the cone was 10 μm with a tip thickness and diameter of 5 and 30 μm , respectively. Glued to the tips of these cones were 1 mm long Cu wires with diameters of 10, 20, and 40 μm . Cu $K\alpha$ emission from the wires was imaged with a Bragg reflection crystal imager⁹ consisting of a 1.6 cm apertured SiO₂ 2131 quartz crystal bent to a radius of 38 cm. The image was reflected at 1.3° off axis and with 15× magnification onto Fujifilm BAS-SR2040 image plates. The view angle was in the horizontal plane at 29.4° from the cone-wire axis. The astigmatism, spherical aberrations, and spherical bending im-

^{a)} Author to whom correspondence should be addressed.

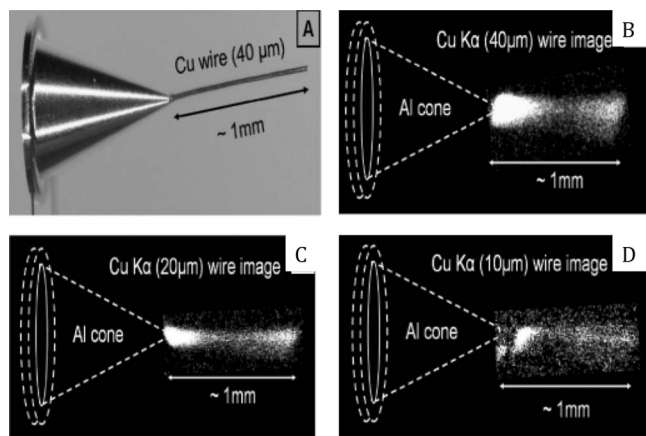


FIG. 1. (a) Picture of a typical target: ~ 1 mm long Cu wire attached to Al cone. Cu $K\alpha$ images of (b) $40\ \mu\text{m}$, (c) $20\ \mu\text{m}$, and (d) $10\ \mu\text{m}$ diameter wire viewed at 29.4° from the wire axis. The aluminum cone is not visible in the images as it does not emit Cu $K\alpha$.

perfections limited the resolution of these images to approximately $20\ \mu\text{m}$. Two other Cu $K\alpha$ diagnostics were employed for each shot: a highly oriented pyrolytic graphite (HOPG) crystal spectrometer¹⁰ and a single hit charge coupled device spectrometer (SHCCD).¹¹ Both spectrometers were tuned to a range of photon energies centered on the Cu $K\alpha$ energy (8.05 keV). At a rear view angle of $\sim 52^\circ$ from the wire axis, the HOPG crystal Bragg reflected x rays onto a Fujifilm BAS-SR2040 image plate. The HOPG spectral bandwidth was limited to ~ 3.5 keV by the length of exposed image plate. The details of the HOPG spectrometer can be found in Ref. 10. The single hit spectrometer consisted of a 2048×2048 pixel, 16 bit, back-thinned, externally cooled Spectral Instruments Series 800 CCD with a pixel size of $13.5\ \mu\text{m}$. The CCD chip was positioned 380 cm from the target chamber center with a front view at 29.8° to the cone-wire axis. Spectra were recorded through a $150\ \mu\text{m}$ Cu filter to ensure single photon counting.

Figure 1 shows examples of the $K\alpha$ images for all three wire diameters (40 , 20 , and $10\ \mu\text{m}$): All such images are typified by an approximately exponential fall off of intensity with about $100\ \mu\text{m}$ scale length from the cone, with a slight increase in emission at the very end of the wire. Absolute $K\alpha$ intensity emission profiles along the wires were found by combining the data from the imager, the SHCCD, and the HOPG spectrometer and by applying sight-line corrections for opacity. The digitized $K\alpha$ images were integrated transverse to the wire axis to generate vertically integrated axial intensity profiles with a typical relative intensity measurement error of $\pm 4\%$. Histograms from the SHCCD exposures were analyzed to provide the number of pixels singly hit by $K\alpha$ photons. By accounting for the CCD quantum efficiency, CCD single hit probability, filter attenuation, and solid angle subtended by the detecting surface, the total Cu $K\alpha$ /sr emitted in the direction of the single hit CCD was found for each shot. There is a significant statistical error of $\pm 50\%$ on these absolute yields and we estimate in addition an absolute accuracy error of $\pm 50\%$.¹²

The relative $K\alpha$ line intensities were obtained from the

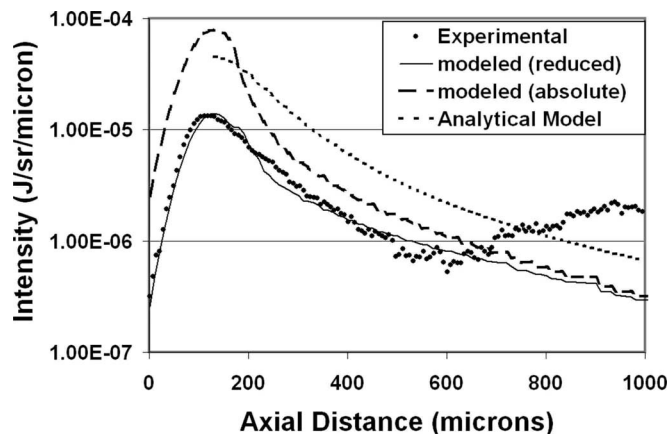


FIG. 2. Experimental and 1D numerically modeled profiles of $K\alpha$ (sr/ μm) vs wire length for the $40\ \mu\text{m}$ diameter wire. The reduced model plot is fitted to the experimental data. The absolute model plot is inferred from the reduced model plot via correction for the temperature dependence of the imager efficiency, as discussed in text.

HOPG spectra by first averaging spectral lines in the spatial direction and then subtracting the background and integrating the digitized image counts in the dispersive direction with a typical measuring error of $\pm 6\%$. A model for opacity correction of Cu $K\alpha$ emitted from a solid copper wire was developed assuming the Cu $K\alpha$ emission energy density within the wire to be radially constant and axially exponential. Opacity correction factors for the imager, HOPG, and SHCCD lines of sight were computed. Axial profile correction factors were derived for application to the experimentally determined $K\alpha$ image profiles and also integrated corrections for the total $K\alpha$ yield from the HOPG and SHCCD. Because the scale length for absorption of Cu $K\alpha$ in Cu is $\sim 25\ \mu\text{m}$, the opacity correction factors were small for the $10\ \mu\text{m}$ wire (1.4) and substantially larger (up to 3.3) for the $40\ \mu\text{m}$ wire.

The HOPG was absolutely calibrated by reference to the SHCCD measurements. An accurate HOPG calibration constant could be determined, in spite of the relatively large SHCCD statistical errors, from the slope of a weighted least-squares linear fit of SHCCD versus HOPG yields. (Specifically, with an uncertainty in the fitted slope of 33%, a statistical uncertainty in a single HOPG measurement of 6%, the resulting statistical uncertainty in a calibrated HOPG yield is 33.5%.) Next, an absolute scaling factor for the measured image intensity was determined as the slope of a weighted linear fit of calibrated HOPG yields versus integrated imager counts. We estimate that this scaling factor has a statistical error of 20%, but an absolute accuracy error of 50%. The experimental profiles were scaled to give axially resolved profiles of $K\alpha$ (sr/ μm). The opacity-corrected $K\alpha$ (sr/ μm) profile of the $40\ \mu\text{m}$ diameter wire is shown in Fig. 2.

We modeled the hot electron transport using a 1D implementation of a previously developed two dimensional numerical code,¹³ which in turn is similar to, but not as complete as, that described by Davies.¹⁴ In this analysis, we are seeking an estimate of the laser energy coupling efficiency into the wire, as well as the self-consistent effective hot electron temperature. We used 1D for simplicity of analysis, fully

aware that our analysis treats the electrons as fluids (thus ignoring the complex motion of the electrons along the wire due to B fields, for example). The simulation starts by assuming a Maxwell–Boltzmann distribution of hot electrons injected axially into the wire: the code then calculates, in small increments along the wire from the injection point, the conversion of electron kinetic energy to heat, as well as to $K\alpha$, and bremsstrahlung emission assuming binary interactions along a straight line path. The simulation requires that the fast electron current is compensated by a cold electron return current; this cold electron current contributes to the heating of the wire through (I^2R) Ohmic losses, as well as creating an (IR) potential that serves to hinder the axial penetration of the hot electrons along the wire. Note that the temperature of the wire was not independently measured but rather computed in each time interval along the wire using the calculated spatial energy density and the published SESAME tabular equation of state.¹⁵ The numerical code generated absolute $K\alpha$ axial emission profiles along the wire as well as axial energy density and temperature profiles. The laser-to-wire coupling efficiency η and the average initial electron temperature T_{hot} were used as free parameters to fit the exponential scale length and absolute intensity of the observed data.

In our model, the resistivity of the wire is approximated as a constant ($10^{-6} \Omega \text{ m}$) for wire temperatures up to 100 eV, then following a Spitzer scaling for greater temperatures. While this is a fair approximation for the temperature dependence of copper resistivity above 10 eV, between room temperature and 10 eV the resistivity of copper increases from approximately $5 \times 10^{-8} \Omega \text{ m}$ to the plateau value of $10^{-6} \Omega \text{ m}$. However, we found that our model simulations of the $K\alpha$ yield and the fitted parameters were quite insensitive to the temperature dependence of the resistivity assumed for less than 10 eV. This is reasonable in that our simulation correctly predicts that there is a pronounced dominance of fast electron collisional heating over Ohmic heating of the return current in the early time portion of the injected current. The collisional heating yields a fast rise in the calculated temperature of the wire to values in excess of 10 eV. Thus the simulation of the $K\alpha$ total yield and axial distribution is expected to be largely independent of the resistivity of copper below 10 eV.

To achieve accurate comparison with the experimental Cu $K\alpha$ profiles, we accounted explicitly for the temperature-dependent efficiency of the Cu $K\alpha$ recording diagnostic. In previous work, we have shown that with increasing temperature of the target, the Cu $K\alpha$ emission line shifts and broadens.¹³ At temperatures reached in this work, the emission line shifts and spreads beyond the crystal bandwidth, reducing the collection efficiency of the imager. This behavior was computed in the numerical code as a reduction in the detected $K\alpha$ emission as a function of the time-varying temperature using correction factors computed from the atomic spectroscopy code FLYCHK.

Figure 2 shows both the results of the numerical code simulations of the axial $K\alpha$ intensity profiles for what is recorded by the temperature-dependent $K\alpha$ imaging system, as well as the absolute (corrected for the diagnostic response)

TABLE I. Comparison of experimental data with transport model results.

Wire diameter (μm)	40	20	10
Electron temperature T_{hot} (keV) (from numerical model fit to data)	750 ± 50	650 ± 50	600 ± 50
Coupling efficiency, η (from numerical model fit to data)	15%	5%	1%
Peak intensity ($K\alpha$) ($\text{sr}/\mu\text{m}$) (proportional to hot electron current)	7.2×10^{-5}	1.5×10^{-5}	4.5×10^{-6}
Peak intensity/area ($K\alpha$) ($\text{sr}/\mu\text{m cm}^2$) (proportional to hot electron current density)	2.7	2.3	2.7
Scale-length (μm) experimental	124	126	63
Scale-length (μm) numerical	97	81	71
Scale-length (μm) analytical	141	88	73

yield. They are plotted together with the experimental profile for the 40 μm diameter wire. The experimental profiles were modified with a blurring to account for the limited spatial resolution at the oblique view angle. The experimental axial emissions were scaled so that the integral of the recorded emission images (corrected for the temperature-dependent efficiency) equaled the total absolute $K\alpha$ yield as determined by techniques described above. Using η and T_{hot} as the free parameters, the numerical model was fitted to the corrected data, yielding the results shown in Table I. Not accounted for in our numerical modeling is the observed $K\alpha$ enhancement at the end of the wire, an artifact most likely the result of electron refluxing, possibly associated with longer scale length surface transport.¹⁶

The computed model profiles were also compared to those from an analytical 1D resistive transport model,¹⁶ which is based on the requirement that the thermal return current density be everywhere equal and opposite to the hot electron current density. In this analytical model, hot electron collisional losses are neglected and the conductivity is constant at the plateau value of $10^6 \Omega^{-1} \text{ m}^{-1}$. In Table I, the predicted $K\alpha$ intensity scale lengths are compared with $K\alpha$ image scale lengths measured in the experiment. Also shown are the electron density scale lengths from the analytical model (where we used the same injected electron beam intensity and temperature found from the fitting of our numerical model to the experimental profiles). The numerical model scale length is in good agreement with that predicted by the analytical model, as well as reasonably reproducing the experimental results.

With the on-target laser energy relatively constant in the experiment ($345 \pm 51 \text{ J}$) and constant in the modeling (345 J), it is not expected that our fitted values for T_{hot} should vary much from shot to shot. This is found in the fits where T_{hot} varies only $\pm 8\%$ from an average of 670 keV (see Table I).

The magnitude of the fitted T_{hot} (750 keV), which is much lower than the value derived from the ponderomotive potential associated with the peak intensity of $2.7 \times 10^{20} \text{ W}/\text{cm}^2$ (6.7 MeV), is a result of forcing our numerical model to fit its parameters to a Maxwell–Boltzmann single temperature distribution (note that small differences in hot electron temperature for three diameter wires are not significant). As succinctly pointed out by Davies,¹⁴ while there

is only modest justification for assuming an analytical “single temperature” electron distribution within materials under these large current conditions, this fitting procedure does give an indication of the mean electron energy. We hasten to observe that this number, which comes from a numerical fit to an electron distribution *within* the material, is not expected to correlate in any simple manner to measurements of electron distributions measured *outside* of the targets with electron spectrometers in vacuum (cf. results in Ref. 17).

The low value of the T_{hot} extracted in the fitting procedure described above, suggests that the mean energy of the injected electrons *in the material* at these very high peak intensities is substantially less than one might have expected from application of conventional ponderomotive scaling. Recent particle in cell modeling¹⁸ has suggested that at these very high intensities light pressure may steepen the density profile and dramatically reduce the relative number of highly energetic electrons compared to those at or near 1 MeV. The origin of this reduction in hot electron energy at high intensities can be seen in recent analytical models¹⁹ in which electrons in the plasma at the critical density surface are driven by the intense electromagnetic fields into the dense plasma to a point well beyond the penetration depth of the light, a lower hot electron temperature is expected. If the T_{hot} value for the generated electron distribution obtained in the modeling of our $K\alpha$ distribution is representative of this departure from ponderomotive scaling, it may help explain the high efficiency of coupling to the imploded plasma in the first FI experiments.³

Finally, the electron conversion efficiency (η) derived from our fitting of the $K\alpha$ distribution is found to scale approximately as the cross sectional area of the wire. Consequently the model predicted peak temperatures due to heating by the electrons are similar (99, 86, and 96 eV) for 40, 20, and 10 μm diameter, respectively. Since a diameter of 40 μm is similar to the required ignition hot spot diameter in FI, our derived value of 15% coupling of the laser energy to this diameter is a rough estimation of the upper limit coupling efficiency via a cone to the ignition hot spot. We note that 15% is close to the 20 % coupling reported in the first integrated FI experiments³ but our conclusion that the cone-wire coupling is proportional to wire area, and that only about 1% couples to a 10 μm wire is in apparent contradiction with the calculation of 6% coupling via a cone to a 5 μm carbon fiber.⁶ Our laser-wire coupling values appear not to be consistent with the results of Baton *et al.*,²⁰ where poor coupling into the flat foil attached to a cone has been observed for 1 μm light. This may be a result of quite different refluxing conditions for the two measurements, and efforts to quantify these differences have begun.²¹

This work was performed under the auspices of the U.S. Department of Energy under Contract Nos. DE-FG02-05ER54834 and W-7405-Eng-48 No. DE-FC02-04ER54789 (Fusion Science Center). J.K. is funded through LLNL’s Institute of Laser Science and Applications grant. We are indebted to Dr. Rod Mason for useful discussions. We would

like to thank the referees for their useful comments, which helped to improve the quality of the paper.

- ¹M. Tabak, J. Hammer, M. E. Glinsky, W. L. Kruer, S. C. Wilks, J. Woodworth, M. Campbell, M. D. Perry, and R. J. Mason, *Phys. Plasmas* **1**, 1626 (1994); M. H. Key, *ibid.* **14**, 055502 (2007).
- ²J. D. Lindl, *Inertial Confinement Fusion* (Springer-Verlag, New York, 1998); M. Rosen, *Phys. Plasmas* **6**, 1690 (1999).
- ³R. Kodama, P. A. Norreys, K. Mima, A. E. Dangor, R. G. Evans, H. Fujita, Y. Kitagawa, K. Krushelnick, T. Miyakoshi, N. Miyanaga, T. Norimatsu, S. J. Rose, T. Shozaki, K. Shigemori, A. Sunahara, M. Tampo, K. A. Tanaka, Y. Toyama, Y. Yamanaka, and M. Zepf, *Nature (London)* **412**, 798 (2001); R. Kodama, H. Shiraga, K. Shigemori, Y. Toyama, S. Fujioka, H. Azechi, H. Fujita, H. Habara, T. Hall, Y. Izawa, T. Jitsuono, Y. Kitagawa, K. M. Krushelnick, K. L. Lancaster, K. Mima, K. Nagai, M. Nakai, H. Nishimura, T. Norimatsu, P. A. Norreys, S. Sakabe, K. A. Tanaka, A. Youssef, M. Zepf, and T. Yamanaka, *ibid.* **418**, 933 (2002).
- ⁴M. H. Key, J. C. Adam, K. U. Akli, M. Borghesi, J. M. H. Chen, R. G. Evans, R. R. Freeman, H. Habara, S. P. Hatchett, J. M. Hill, A. Heron, J. A. King, R. Kodama, K. L. Lancaster, A. J. Mackinnon, P. Patel, T. Phillips, L. Romagnani, R. A. Snavely, R. Stephens, C. Stoeckl, R. Town, Y. Toyama, B. Zhang, M. Zepf, and P. A. Norreys, *Phys. Plasmas* **15**, 022701 (2008).
- ⁵S. Atzeni, A. Schiavi, and C. Bellei, *Phys. Plasmas* **14**, 052702 (2007).
- ⁶R. Kodama, Y. Sentoku, Z. L. Chen, G. R. Kumar, S. P. Hatchett, Y. Toyama, T. E. Cowan, R. R. Freeman, J. Fuchs, Y. Izawa, M. H. Key, Y. Kitagawa, K. Kondo, T. Matsuoka, H. Nakamura, M. Nakatsutsumi, P. A. Norreys, T. Norimatsu, R. A. Snavely, R. B. Stephens, M. Tampo, K. A. Tanaka, and T. Yabuuchi, *Nature (London)* **432**, 1005 (2004).
- ⁷S. C. Wilks, W. L. Kruer, M. Tabak, and A. B. Langdon, *Phys. Rev. Lett.* **69**, 1383 (1992).
- ⁸C. N. Danson, J. Collier, D. Neely, L. J. Barzanti, A. Damerell, C. B. Edwards, M. H. R. Hutchinson, M. H. Key, P. A. Norreys, D. A. Pepler, I. N. Ross, P. F. Taday, W. T. Toner, M. Trentelman, F. N. Walsh, T. B. Winstone, and R. W. W. Wyatt, *J. Mod. Opt.* **45**, 1653 (1998).
- ⁹J. A. Koch, O. L. Landen, T. W. Barbee, P. Celliers, L. B. Da Silva, S. G. Glendinning, B. A. Hammel, D. H. Kalantar, C. Brown, J. Seely, G. R. Bennett, and W. Hsing, *Appl. Opt.* **37**, 1784 (1998).
- ¹⁰A. Pak, G. Gregori, J. Knight, K. Campbell, D. Price, B. Hammel, O. L. Landen, and S. H. Glanzer, *Rev. Sci. Instrum.* **75**, 3747 (2004).
- ¹¹C. Stoeckl, W. Theobald, T. C. Sangster, M. H. Key, P. Patel, B. Zhang, R. Clarke, S. Karsch, and P. Norreys, *Rev. Sci. Instrum.* **75**, 3705 (2004).
- ¹²W. Theobald, personal communication (10 April 2007).
- ¹³K. U. Akli, M. H. Key, H. K. Chung, S. B. Hansen, R. R. Freeman, M. H. Chen, G. Gregori, S. Hatchett, D. Hey, N. Izumi, J. King, J. Kuba, P. Norreys, A. J. Mackinnon, C. D. Murphy, R. Snavely, R. B. Stephens, C. Stoeckel, W. Theobald, and B. Zhang, *Phys. Plasmas* **14**, 023102 (2007).
- ¹⁴J. R. Davies, *Phys. Rev. E* **65**, 026407 (2002).
- ¹⁵S. P. Lyon and J. D. Johnson, “SESAME: The Los Alamos National Laboratory Equation of State Database,” Los Alamos National Laboratory Technical Report No. LA-UR-92-3407, 1992.
- ¹⁶A. R. Bell, J. R. Davies, S. Guerin, and H. Ruhl, *Plasma Phys. Controlled Fusion* **39**, 653 (1997).
- ¹⁷T. E. Cowan, A. W. Hunt, T. W. Phillips, S. C. Wilks, M. D. Perry, C. Brown, W. Fountain, S. Hatchett, J. Johnson, M. H. Key, T. Parnell, D. M. Pennington, R. A. Snavely, and Y. Takahashi, *Phys. Rev. Lett.* **84**, 903 (2000); H. Habara, K. Azumi, T. Yabuuchi, T. Nakamura, Z. L. Chen, M. Kashihara, R. Kodama, K. Kondo, G. R. Kumar, L. A. Lei, T. Matsuoka, K. Mima, and K. A. Tanaka, *ibid.* **97**, 095004 (2006).
- ¹⁸B. Chrisman, Y. Sentoku, and A. J. Kemp, *Phys. Plasmas* **15**, 056309 (2008); A. J. Kemp, Y. Sentoku, and M. Tabak, *Phys. Rev. Lett.* **101**, 075004 (2008).
- ¹⁹M. G. Haines, M. S. Wei, F. N. Beg, and R. B. Stephens, *Phys. Rev. Lett.* **102**, 045008 (2009).
- ²⁰S. D. Baton, M. Koenig, J. Fuchs, A. Benuzzi-Mounaix, P. Guillou, B. Loupias, T. Vinci, L. Gremillet, C. Rousseaux, M. Drouin, E. Lefebvre, F. Dorchie, C. Fourment, J. J. Santos, D. Batani, A. Morace, R. Redaelli, M. Nakatsutsumi, R. Kodama, A. Nishida, N. Ozaki, T. Norimatsu, Y. Aglitskiy, S. Atzeni, and A. Schiavi, *Phys. Plasmas* **15**, 042706 (2008).
- ²¹S. D. Baton, personal communication (12 Nov 2008).